Stefan Rönsch[1,2]
Jakob Köchermann[1]
Jens Schneider[1]
Steffi Matthischke[1]

[1]Deutsches Biomasseforschungszentrum gemeinnützige GmbH, Leipzig, Germany.

[2]Ernst-Abbe-Hochschule Jena, Jena, Germany.

Global Reaction Kinetics of CO and CO_2 Methanation for Dynamic Process Modeling

For the design and optimization of methfanation processes detailed modeling and simulation work is advisable. However, only a few kinetics published in literature rely on wide temperature and pressure ranges, which are prevalent at modern methanation applications with dynamic operation. Especially the simulation-based design of methanation processes with commercial catalysts is difficult due to legal restrictions regarding the publication of kinetic data of those catalysts. In this work, rate equations for the dynamic modeling and simulation of methanation processes operating with commercial Ni/Al_2O_3 catalysts are selected, adapted, and tested in a dynamic reactor model. The results suggest that the catalyst's nickel content is an indicator for the choice of a rate equation. Testing of the equations in a reactor model meets published data for CO and CO_2 methanation and own measurements.

Keywords: Dynamic model, Kinetics, Methanation, Power to gas, Syngas

Received: June 09, 2015; *revised:* August 07, 2015; *accepted:* December 01, 2015

DOI: 10.1002/ceat.201500327

1 Introduction

In current energy research, the catalytic synthesis of methane (methanation) draws significant attention as a connector of electricity and natural gas grid (cf. Fig. 1) [1, 2]. Two options, CO_2 (Eq. (1)) and CO methanation (Eq. (2)), are discussed in this context:

$$CO_2 + 4H_2 \rightleftharpoons CH_4 + 2H_2O \quad -164\,kJ\,mol^{-1}(at\,298\,K) \quad (1)$$

$$CO + 3H_2 \rightleftharpoons CH_4 + H_2O \quad -206\,kJ\,mol^{-1}(at\,298\,K) \quad (2)$$

The first option, the so-called CO_2 methanation, is operated with CO_2 and hydrogen as educts for methane production. Thereby, the use of electrolysis hydrogen provides the possibility for a chemical (methane-based) storage of surplus electricity [3].

As second option, methanation processes for the upgrading of CO-rich gases (e.g., from biomass or coal gasification) are discussed (CO methanation). At present, this process is especially used to produce Bio-SNG (Bio Synthetic Natural Gas) as a fuel with low greenhouse gas emissions in comparison to fossil natural gas [4].

To meet the demands of the changing energy system, e.g., integration of fluctuating wind and solar energy, both process options are related to challenging operation conditions. Amongst others, a flexible operation of the methanation process regarding the syngas input flow and the operation temperature has to be ensured [5, 6]. Consequently, attention is paid to detailed modeling and simulation work aiming at the design and optimization of flexible methanation processes. For that purpose, a multitude of kinetic approaches for the CO methanation on nickel catalysts were published within the last decades. However, for wide temperature and pressure ranges (i.e., 250–900 °C, 5–30 bar) typically appearing at a flexible methanation operation of chemical storage systems, the majority of those kinetic approaches does not lead to satisfying results. Due to legal restrictions regarding the publication of kinetic data for commercial catalysts, especially the simulation-based design and optimization of methanation pilot plants operating with commercial Ni/Al_2O_3 catalysts is difficult.

Therefore, it is the aim of this work to select, adapt, and test appropriate rate equations for the dynamic modeling and simulation of methanation processes operating with commercial Ni/Al_2O_3 catalysts. For that purpose, first the current state of research on methanation applications, kinetics, and dynamic modeling is described. On this basis, different rate equations for dynamic methanation modeling are analyzed, selected, adapted, and validated by own measurements. Finally, the adapted rate equations are tested in a 1D reactor model for a dynamic simulation of the methanation process. Mechanisms concerning catalyst deactivation, e.g., sulfur poisoning or carbon formation by the Boudouard reaction, are neglected.

2 State of Research

An overview about research on methanation applications, kinetics, and the use of reaction rates for dynamic methanation modeling is given in the following.

Correspondence: Prof. Dr. Stefan Rönsch (stefan.roensch@dbfz.de), Deutsches Biomasseforschungszentrum gemeinnützige GmbH, Torgauer Straße 116, 04347 Leipzig, Germany.

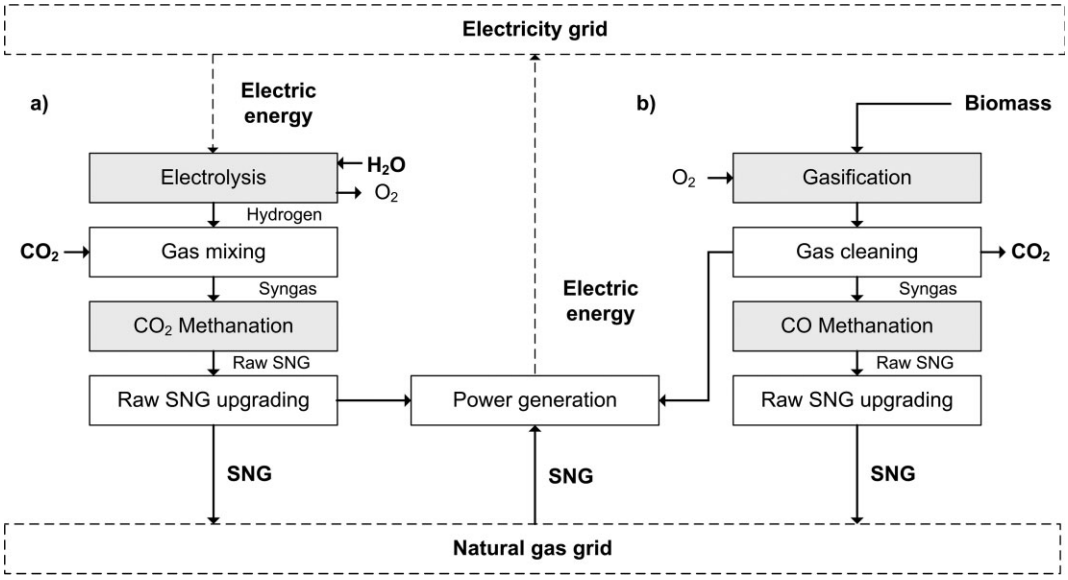

Figure 1. Methanation plants for flexible power generation as connectors of electricity and natural gas grid: (a) electrolysis-based process with CO_2 methanation; (b) gasification-based process with CO methanation.

2.1 Methanation Applications

Research activities on methanation processes and kinetics go back to the beginning of the 20th century. After the first publication by Sabatier and Senderens [7] in 1902, the CO methanation over nickel surfaces was intensively investigated for the syngas cleaning upstream ammonia synthesis and for the use of gas from coal gasification systems [8]. Especially during the oil crisis in the late 1970s and 1980s, research expenditures on methanation of CO-containing coal gas increased and different methanation processes came to commercial maturity. An overview of this development is given by Kopyscinski [9] and Rönsch [10]. Research on CO_2 methanation played a minor role in the 20th century. Only a few studies investigated this process, e.g., for the use of coke oven and/or blast furnace gas [11, 12]. Due to a comparatively high effort related to gas compression and gas cleaning, the use of these CO_2-containing methanation educts did not succeed at a commercial scale [13].

Within the scope of reducing anthropogenic greenhouse gas emissions, at the beginning of the 21th century research on methanation was resumed. Now, instead of gas produced from coal, syngases from biomass gasification are in the focus of CO methanation in flexible polygeneration plants [14, 15]. Besides this, electrolysis hydrogen mixed with CO_2 gains importance and provides a new opportunity as educt for CO_2 methanation and for connecting the gas and electricity grid (Fig. 1) [3, 16]. For both applications, CO methanation in polygeneration plants and CO_2 methanation of electrolysis hydrogen, a flexible (dynamic) operation of the methanation is prevalent and requires detailed process modeling and simulation in wide pressure and temperature ranges. Intensive investigations are currently carried out [1, 5, 6, 17, 18].

2.2 Methanation Kinetics

According to the peak of methanation process development in the 1970s and 1980s, a multitude of kinetic approaches for CO methanation was published in this time. The publications differ by the catalytic material (commercial and noncommercial nickel-containing catalysts) temperature ranges, pressure ranges, test equipment (differential or integral reactors), catalyst size, and kinetic models (power law or Langmuir-Hinshelwood). Overviews of kinetic approaches published for CO methanation are given by Kopyscinski [19], Mills et al. [20], Klose [21], and Vannice et al. [22].

Due to the lack of commercial applications, kinetics for CO_2 methanation can be rarely found in literature from the 1970s and 1980s. Publications from Kaltenmaier [11], Xu [23], and Weatherbee [12] are three examples for studies regarding CO_2 methanation kinetics in that time. Instead of determining special rate equations for CO_2 methanation, different authors complement CO methanation kinetics by kinetics of the reverse water-gas shift reaction, e.g., [19, 23]. Thereby, CO_2 methanation is seen as a linear combination of CO methanation and reverse water-gas shift reaction.

Among the kinetic data for CO methanation mentioned by Kopyscinski [19] and Mills [20], only seven approaches are determined at elevated pressures (> 2 bar), which are typical for modern methanation plants. Four of them deal with commercial nickel catalysts characterized by nickel contents of 15, 18, 22, and 50 %. Tab. 1 gives an overview of these kinetic studies.

Already in 1969, Schoubye [24] from Haldor Topsoe published a simplified Langmuir-Hinshelwood kinetic for CO methanation over a $Ni/MgAl_2O_4$ catalyst. He considered pressures between 1 and 15 bar and temperatures between 200 °C and 294 °C for the respective catalyst in a fluidized-bed reactor. More than ten years later, in 1980, Ho and Harriot [30] studied the kinetics of a 2 and 10 % nickel catalyst under elevated pres-

Table 1. Studies investigating CO methanation (and reverse water-gas shift) kinetics at elevated pressures.

Author/year	Catalyst	Pressure/temperature	Reactor/diameter	Kinetic approach	Reactions
Schoubye/1969 [24]	$Ni/MgAl_2O_4$ (9–10 % Ni) and others	1–15 atm/200–294 °C	Fluidized-bed/8.0 mm	Langmuir-Hinshelwood	Co methanation
Sughrue/1982 [25]	Ni/Al_2O_3 (5 % Ni) [b]	27.6 bar/200–350 °C	Berty	Langmuir-Hinshelwood	CO methanation
Klose/1984 [26]	Ni/Al_2O_3 (18 % Ni) [a]	20–30 bar/180–284 °C	Berty	Langmuir-Hinshelwood	CO methanation, C_2H_4 formation
Hayes/1985 [27]	Ni/Al_2O_3 (9 % Ni, 1.5 % Pt)	1–5 bar/260–300 °C	Fixed-bed/9.5 mm	Power law	CO methanation
Chen/1988 [28]	Ni/Al_2O_3 (n.s.) [a),c)]	1–34 atm/230–300 °C	Berty	Power law	CO methanation
Xu/1989 [23]	$Ni/MgAl_2O_4$ (15.2 % Ni) [a]	3–10 bar/300–400 °C	Fixed-bed/10.7 mm	Langmuir-Hinshelwood	CO methanation, CO_2 methanation, WGS
Zhang/2013 [29]	Ni/Al_2O_3 (50 % Ni) [a]	1–5 bar/250–360 °C	Fixed-bed in copper block/1.4 mm	Langmuir-Hinshelwood	CO methanation, WGS

[a)]commercial; [b)]in Ni/Al_2O_3 coating on monolithic structure; [c)]Haldor Topsoe MCR-2X.

sures up to 3 bar. They proposed a rate equation, however, without publishing the preexponential factor.

In 1982, Sughrue and Bartolomew [25] published a Langmuir-Hinshelwood kinetic measured at 6.9 bar between 200 °C and 350 °C in a Berty reactor with a Ni/Al_2O_3 catalyst. For the first time, Sughrue tried to integrate data from other studies into his work and to compare it with own measurements. It was his aim to provide a kinetic approach covering a broad temperature range.

In 1984, Klose and Baerns [26] investigated CO methanation over a commercial Ni/Al_2O_3 catalyst in a Berty reactor. Their investigations covered pressures between 1 and 25 bar and temperatures between 180 °C and 284 °C. As kinetic approach they proposed a Langmuir-Hinshelwood kinetic. Kinetics for the reverse water-gas shift reaction and CO_2 methanation were neglected by Klose and Baerns.

In contrast, 1985 Hayes and co-workers [27] proposed a power law kinetic for Ni/Al_2O_3 catalysts. The kinetic resulted from measurements at a fixed-bed reactor at pressures between 1 and 5 bar and temperatures between 260 °C and 300 °C. Three years later, in 1988, Chen [28] investigated the kinetics of the commercial methanation catalyst MCR-2X from Haldor Topsoe. He used a Berty reactor and covered pressures between 1 and 34 atm in a temperature range between 230 °C and 300 °C.

In 1989, Xu and Froment [23] published their work 'Methane Steam Reforming, Methanation and Water-Gas Shift', which comprises rates of reaction for methane steam reforming, methanation, and water-gas shift over a commercial 15 % nickel catalyst. Regarding the methanation reaction, they investigated pressures between 3 and 10 bar as well as comparatively high temperatures between 300 °C and 400 °C in a fixed-bed reactor.

Finally, in 2013, Zhang and co-authors [29] came out with a work on the kinetics of a commercial 50 % nickel catalyst in a micro fixed-bed reactor with a diameter of 1.4 mm. Zhang adapted the rate equations from Xu [23] and Klose [26] to his own measurements between 1 and 5 bar and 250 °C and 360 °C. Beside Xu and Froment [23], Zhang is the only author listed in Tab. 1 who paid attention to the reverse water-gas shift reaction which is crucial to model CO_2 methanation processes.

2.3 Use of Reaction Rates for Methanation Dynamic Modeling

Current dynamic simulations of CO and CO_2 methanation processes primarily refer to rates from Xu [23], e.g., [17, 31], and with less frequency to the rates determined by Kopyscinski [19], e.g., [32]. However, a closer look at these models and reaction rates reveals a significant validity limitation concerning the methanation temperature. As an example, the rates for CO methanation published by Xu and Kopyscinski are given in Fig. 2 for an exemplary gas composition given by Harms [33].

The curves in Fig. 2 show the typical shape of methanation rates over temperature. Negative values indicate that CO is reduced by the methanation reaction (methane formation). The CO reduction increases with temperature until the reaction switches from methane formation to methane reforming. Thereby, the change from methane formation to reforming is characterized by a distinctive minimum of the curve.

Furthermore, Fig. 2 discloses the problems with the rates given by Xu [23] and Kopyscinski [19] for the dynamic simulation of methanation processes in wide temperature ranges. While the rate proposed by Xu at temperatures below 700 K is almost inactive, the rate proposed by Kopyscinski is characterized by a too intense reverse reaction (methane reforming) at temperatures above 650 K. This feature becomes obvious by changing the axis scaling of Fig. 2 to 0 and $-2\,mol\,CO\,kg^{-1}cat.\,s^{-1}$, which is done at the lower left side of Fig. 2.

The reason for this inappropriate behavior is the temperature range at which the rates of reaction were determined. Xu

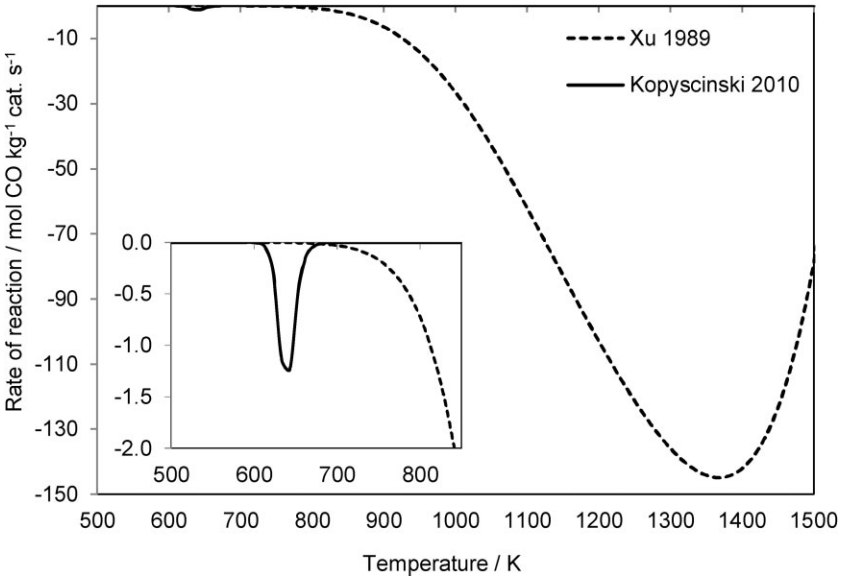

Figure 2. Reaction rate of CO methanation calculated based on Xu [23] and Kopyscinski [19] at $p = 27.2$ bar, $y_{CO} = 0.0984$, $y_{N2} = 0.0440$, $y_{H2} = 0.6545$, $y_{CO2} = 0.0896$, $y_{CH4} = 0.1130$, $y_{H2O} = 0.0005$ [33].

focused at methane reforming typically occurring at temperatures above 900 K. In contrast, Kopyscinski measured kinetics around 573 K under atmospheric conditions in order to apply them to a proximate isothermal fluidized-bed methanation reactor.

3 Rate analysis, Selection, and Adaption

As described above, an appropriate kinetic approach for the modeling and simulation of dynamic (unsteady) CO and CO_2 methanation processes has to pay attention to wide operation temperature and pressure ranges. However, only a few kinetics take these requirements into account and may lead to unrealistic results. Therefore, a theoretical analysis of published methanation kinetics for commercial Ni/Al_2O_3 catalysts is presented in the following. Based on this, rate equations that seem to be suitable for the modeling and simulation of dynamic methanation processes are selected and adapted. Finally, these rate equations are validated with own measurements.

3.1 Theoretical Analysis

Results from dynamic methanation models using kinetics from Xu [23] and Kopyscinski [19] (cf. Sect. 2.3) underline the importance of appropriate rate equations especially for the dynamic simulation of methanation with commercial nickel catalysts.

Regarding the kinetics mentioned in Tab. 1, four studies investigated commercial nickel catalysts:

- Chen [28] published a kinetic approach for the Haldor Topsoe MCR-2X catalyst, which is reported by Rostrup-Nielsen et al. [34] to contain 22 % nickel.
- Xu [23] did experiments with a commercial 15 % nickel catalyst.
- Klose [26] analyzed a catalyst with 18 % nickel.
- Zhang [29] tested a catalyst with 50 % nickel.

Due to confidentiality reasons, there is little information available about the MCR-2X catalyst. Thus, an analysis of reaction rates for the dynamic modeling of methanation processes is not possible for that catalyst in this work. However, authors from Haldor Topsoe, e.g., in [34], refer to rates from Schoubye [24] or Sehested [35] for catalyzed methanation. The catalyst investigated by Xu is a special steam reforming catalyst. Therefore, and due to the limited activity at lower (methanation-typical) temperatures (cf. Fig. 2), this catalyst also is not considered in this work.

In recent studies concerning methanation over commercial Ni/Al_2O_3 catalysts, increasingly catalysts with 18 % and 50 % nickel are mentioned. As written above, corresponding rates of reaction for these catalysts are published by Klose and Zhang. Both rates are plotted together with the rates from Xu and Kopyscinski in Fig. 3. In contrast to the rates of Xu and Kopyscinski, the rates reported by Klose and Zhang show reasonable values suitable for reactor modeling and simulation, i.e., no dominant methane reforming, observable methanation activity at temperatures around 573 K, even at temperatures below 700 K.

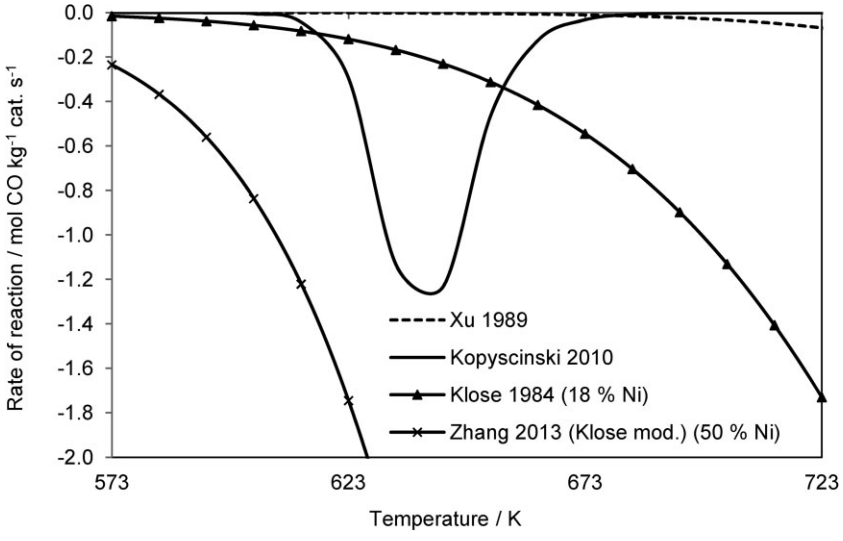

Figure 3. Reaction rates of CO methanation calculated based on Xu [23], Kopyscinski [19], Klose [26], and Zhang [29] at $p = 27.2$ bar, $y_{CO} = 0.0984$, $y_{N2} = 0.0440$, $y_{H2} = 0.6545$, $y_{CO2} = 0.0896$, $y_{CH4} = 0.1130$, $y_{H2O} = 0.0005$ [33].

The nickel contents of these catalysts fit very well to that of commercial catalysts from Clariant and CRI Catalyst Leuna, respectively. Therefore, based on the theoretical analysis in this work, the application of the rates from Klose and Zhang is recommended to model methanation processes with those commercial 18 % and 50 % nickel catalysts.

Regarding CO_2 methanation, an appropriate rate for the reverse water-gas shift reaction has to be found in addition to a rate for CO methanation; both rates are applied as a linear combination. However, only a few authors report rates of this reaction together with CO methanation over nickel catalysts. Among the authors listed in Tab. 1, only Xu and Zhang published rates for the reverse water-gas shift reaction. Both rates are displayed in Fig. 4 together with the rates for CO methanation from Klose and Zhang.

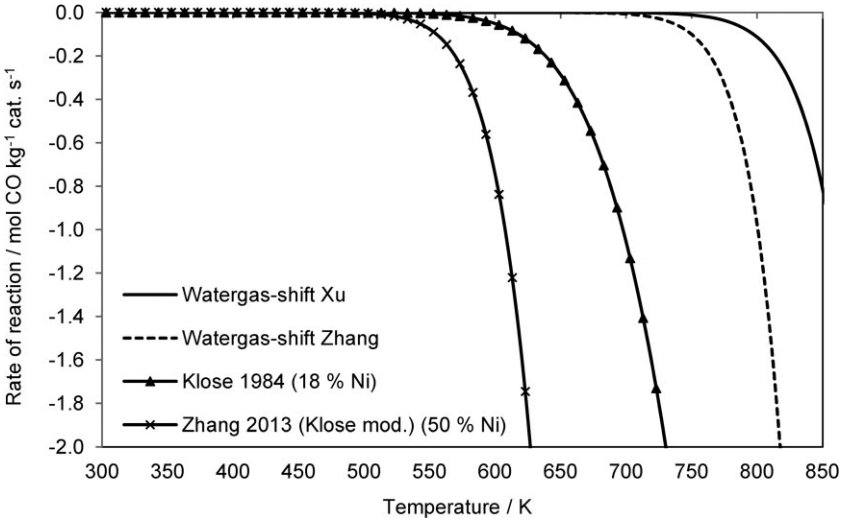

Figure 4. Reaction rates of CO methanation calculated based on Xu [23] and Klose [26] and reverse water-gas shift reaction based on Xu [23] and Zhang [29] at $p = 27.2$ bar, $y_{CO} = 0.0984$, $y_{N2} = 0.0440$, $y_{H2} = 0.6545$, $y_{CO2} = 0.0896$, $y_{CH4} = 0.1130$, $y_{H2O} = 0.0005$ [33].

Fig. 4 indicates less reverse water-gas shift activity than CO methanation activity in the analyzed temperature range. Besides, a lower reverse water-gas shift activity for rates published by Xu in comparison to the rates published by Zhang is obvious. This is important especially at temperatures below 850 K, which are typical for CO_2 methanation processes. While calculations based on a linear combination of a rate for CO methanation and the reverse water-gas shift rate given by Xu do not meet actual reports of CO_2 methanation experiments (cf. [16, 36]), respective calculations based on rates for CO methanation and reverse water-gas shift given by Zhang agree with current measurements; see Sect. 4. Calculations based on rates for CO methanation and reverse water-gas shift from Xu result in a significantly too low CO_2 methanation activity.

3.2 Rate Selection and Adaption

According to Sect. 3.1, rates from Klose and Zhang should be applied to model CO methanation processes over wide temperature ranges. For modeling and simulation CO_2 methanation processes, a linear combination of CO methanation and reverse water-gas shift reaction is suitable. Therefore, the rate equations published by Zhang for reverse water-gas shift and CO methanation reaction and/or Klose for CO methanation seem to be appropriate (as explained in Sect. 3.1; cf. Fig. 4).

While Klose suggested a rate equation for the CO methanation over a commercial 18 % nickel catalyst (Eq. (3)), Zhang published rate equations for CO methanation (Eq. (4)) and watergas-shift reaction (Eq. (5)) over commercial 50 % nickel catalysts. Concerning the rate for CO methanation, Zhang adapted the formula given by Klose by changing the preexponential factor used to calculate k_1[1)]. For the reverse water-gas shift reaction, Zhang modified an equation originally coming from Xu.

$$r_{\mathrm{METH,18\%Ni}} = -\frac{k_{1,\mathrm{Klose}}\, K_C\, K_H^2\, p_{CO}^{0.5}\, p_{H_2}}{\left(1 + K_C\, p_{CO}^{0.5} + K_H\, p_{H_2}^{0.5}\right)^3} \tag{3}$$

$$r_{\mathrm{METH,50\%Ni}} = -\frac{k_{1,\mathrm{Zhang}}\, K_C\, K_H^2\, p_{CO}^{0.5}\, p_{H_2}}{\left(1 + K_C\, p_{CO}^{0.5} + K_H\, p_{H_2}^{0.5}\right)^3} \tag{4}$$

$$r_{\mathrm{WGS}} = \frac{\frac{k_2}{p_{H_2}}\left(p_{CO}\, p_{H_2O} - \frac{p_{H_2}\, p_{CO_2}}{K_{\mathrm{WGS}}}\right)}{\left(1 + K_{CO}\, p_{CO} + K_{H_2}\, p_{H_2} + K_{CH_4}\, p_{CH_4} + \frac{K_{H_2O}\, p_{H_2O}}{p_{H_2}}\right)} \tag{5}$$

To use the selected rates from Klose and Zhang in a reactor model for the simulation of dynamic methanation (i.e., operation with wide and changing variables of state), the rate equations were adapted (Eqs. (6) to (8)). In this context it is important to complement the rate equations of CO methanation by a term characterizing the reverse reaction (methane reforming) occurring at elevated temperatures. The reverse reaction is essential to ensure the calculation of equilibrium values at sufficient gas residence times in the methanation reactor. Regarding the reverse water-gas shift reaction, it has to be noticed that Zhang adapted the rate equation from Xu, however, did not take the exponent of the adsorption term (denominator) into account. This and minor mistakes related to the units of the kinetic parameters are corrected here (cf. Eqs. (5) and (8)).

$$r_{\mathrm{METH,18\%Ni}} = -\frac{k_{1,\mathrm{Klose}}\, K_C\, K_H^2\, p_{CO}^{0.5}\, p_{H_2}}{\left(1 + K_C\, p_{CO}^{0.5} + K_H\, p_{H_2}^{0.5}\right)^3} + \frac{k_{1,\mathrm{Klose}}\, K_C\, K_H^2\, p_{CH_4}\, p_{H_2O}\, p_{CO}^{-0.5}\, p_{H_2}^{-2}\left(\frac{1}{K_{\mathrm{METH}}}\right)}{\left(1 + K_C\, p_{CO}^{0.5} + K_H\, p_{H_2}^{0.5}\right)^3} \tag{6}$$

1) List of symbols at the end of the paper.

$$r_{\mathrm{METH,50\%Ni}} = -\frac{k_{1,\mathrm{Zhang}}\, K_{\mathrm{C}}\, K_H^2\, p_{\mathrm{CO}}^{0.5}\, p_{\mathrm{H_2}}}{\left(1 + K_{\mathrm{C}}\, p_{\mathrm{CO}}^{0.5} + K_{\mathrm{H}}\, p_{\mathrm{H_2}}^{0.5}\right)^3} + \frac{k_{1,\mathrm{Zhang}}\, K_{\mathrm{C}}\, K_{\mathrm{H}}^2\, p_{\mathrm{CH_4}}\, p_{\mathrm{H_2O}}\, p_{\mathrm{CO}}^{-0.5}\, p_{\mathrm{H_2}}^{-2}\left(\frac{1}{K_{\mathrm{METH}}}\right)}{\left(1 + K_{\mathrm{C}}\, p_{\mathrm{CO}}^{0.5} + K_{\mathrm{H}}\, p_{\mathrm{H_2}}^{0.5}\right)^3} \quad (7)$$

$$r_{\mathrm{WGS}} = \frac{\frac{k_2}{p_{\mathrm{H_2}}}\left(p_{\mathrm{CO}}\, p_{\mathrm{H_2O}} - \frac{p_{\mathrm{H_2}}\, p_{\mathrm{CO_2}}}{K_{\mathrm{WGS}}}\right)}{\left(1 + K_{\mathrm{CO}}\, p_{\mathrm{CO}} + K_{\mathrm{H_2}}\, p_{\mathrm{H_2}} + K_{\mathrm{CH_4}}\, p_{\mathrm{CH_4}} + \frac{K_{\mathrm{H_2O}}\, p_{\mathrm{H_2O}}}{p_{\mathrm{H_2}}}\right)^2} \quad (8)$$

The rate coefficients k_1 and k_2 in Eqs. (6) to (8) are calculated by Eq. (9), where the index j denotes the reactions: $j = 1$ for CO methanation, $j = 2$ for reverse water-gas shift reaction. Eq. (10) defines the adsorption constants appearing in Eqs. (6) to (8). The index n describes the adsorbed species C, H, CO, H_2, CH_4, and H_2O.

$$k_{\mathrm{j}} = k_{\mathrm{j}}^0 \exp(-E_{\mathrm{n}}/RT_{\mathrm{G}}) \quad (9)$$

$$K_{\mathrm{n}} = K_{\mathrm{n}}^0 \exp(-\Delta H_{\mathrm{n}}/RT_{\mathrm{G}}) \quad (10)$$

The kinetic parameters of Eqs. (9) and (10) are given in Tab. 2.

Table 2. Kinetic parameters of Eqs. (9) and (10).

Symbol	Value
$k_{1,\mathrm{Klose}}^0$ [mol kg^{-1}cat s^{-1}]	$(4.8/3.6)\times10^9$
$k_{1,\mathrm{Zhang}}^0$ [mol kg^{-1}cat s^{-1}]	$(7.0/3.6)\times10^{10}$
k_2^0 [mol kg^{-1}cat s^{-1}bar^{-1}]	$(7.83/3.6)\times10^6$
E_1 [J mol^{-1}]	103 000
E_2 [J mol^{-1}]	62 000
K_{C}^0 [bar$^{-0.5}$]	5.8×10^{-4}
K_{H}^0 [bar$^{-0.5}$]	1.6×10^{-2}
K_{CO}^0 [bar^{-1}]	8.23×10^{-5}
$K_{\mathrm{H_2}}^0$ [bar^{-1}]	6.12×10^{-9}
$K_{\mathrm{CH_4}}^0$ [bar^{-1}]	6.65×10^{-4}
$K_{\mathrm{H_2O}}^0$ [–]	1.77×10^5
ΔH_{C} [J mol^{-1}]	–42 000
ΔH_{H} [J mol^{-1}]	–16 000
ΔH_{CO} [J mol^{-1}]	–70 650
$\Delta H_{\mathrm{H_2}}$ [J mol^{-1}]	–82 900
$\Delta H_{\mathrm{CH_4}}$ [J mol^{-1}]	–38 280
$\Delta H_{\mathrm{H_2O}}$ [J mol^{-1}]	88 680

3.3 Experimental Validation

In order to validate the conclusions drawn above, the rates proposed for 18 % and 50 % nickel catalysts were compared with own basic measurements (cf. [37]). An electrically heated fixed-bed reactor with an internal diameter of 13 mm and a length of 184 mm was used. Inside the reactor a catalyst bed with a height of 5 mm and an overall mass of 0.4 g was integrated. The diameter of the catalyst particles was in between 0.5 and 1.0 mm. The catalyst layer was embedded by two layers of inert Al_2O_3 spheres for the homogenization of the gas flow (Fig. 5). All experiments were conducted at a constant catalyst temperature of 400 °C, atmospheric pressure, and with a flow rate of 60 L h^{-1} (standard temperature and pressure, STP). The educt gas was mixed and provided by mass flow controllers (MFCs) for CO, H_2, and N_2. A gas composition of 18.75 vol % H_2, 6.25 vol % CO, and 75.0 vol % N_2 was passed from the bottom-up through the reactor. Both educt gas and product gas were analyzed by the microgas chromatograph GCM® Microbox II (μ-GC) for permanent gases made by Elster. Therewith, N_2, H_2, CO, CO_2, and CH_4 concentrations were measured.

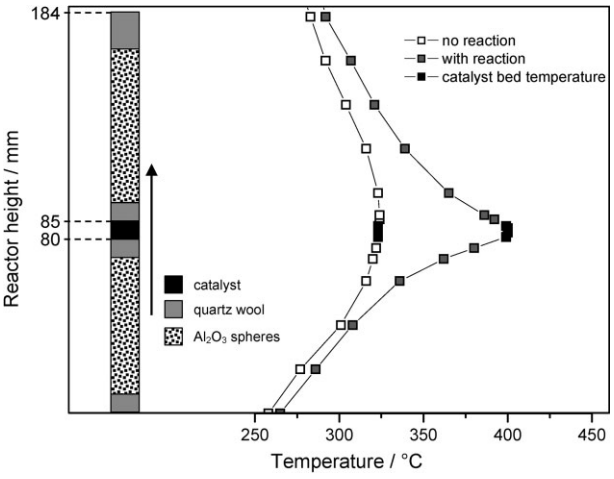

Figure 5. Reactor charge and temperature profile for experimental rate determination at atmospheric pressure (with and without reaction).

The catalysts were activated with hydrogen. Therefore, a gas mixture consisting of 10 vol % H_2 in nitrogen was passed through the reactor for 6 h. During this time, the reactor was heated from ambient temperature up to a temperature of 320 °C. This temperature was held for 1 h. After the activation, the reactor was cooled down again to ambient temperature.

All experiments started with heating the fixed-bed reactor at a heating rate of 280 K h^{-1}. During the heating process, an inert volume flow of N_2 passed the reactor. The educt gas was added when the catalyst bed reached a temperature of 320 °C. A steady-state catalyst temperature of 400 °C was reached by regulating the heating furnace. The axial temperature variation in the center of the fixed catalyst bed was within 2 K at steady state (Fig. 5). It was determined by a moveable thermocouple located in a fixed and sealed pipe in the middle of the bed.

At 400 °C and atmospheric pressure, a reaction rate of about 0.0722 mol kg^{-1}cat. s^{-1} for the 50 % nickel catalyst was observed. In contrast, the 18 % nickel catalyst showed a rate of reaction of approximately 0.0639 mol kg^{-1}cat. s^{-1}. The measurements do not meet the exact values calculated by the rates of Klose (0.0196 mol kg^{-1}cat. s^{-1}) and Zhang (0.2864 mol kg^{-1}cat. s^{-1}). However, they confirm the assumption that the rate published by Klose is more suitable for modeling methanation processes with a commercial 18 % nickel catalyst (to be characterized by a lower rate) and the rates reported by Zhang should be used for processes with a commercial 50 % nickel catalyst (to be characterized by a higher rate). Although for practical applications almost irrelevant due to the fast reaction, it was approved by the measurements that 18 % nickel catalysts and rates from Klose show a slightly lower methanation activity than 50 % nickel catalysts and rates from Zhang.

4 Rate Application

Rates of reaction are commonly used in simulation models aiming at the design and/or upscaling of methanation reactors. To emphasize the possibilities of the rates selected in Sect. 3.2, they are exemplarily used in a simplistic dynamic fixed-bed methanation reactor model with an 18 % nickel catalyst.

4.1 Reactor Modeling

The fixed-bed methanation reactor is modeled with the software package Octave. It is represented by a pseudo-homogeneous 1D plugged-flow model described in [38]. The model relies on a system of seven differential equations: the energy balance of the gas (Eq. (11)) and the component balances of the gas species CO, N_2, H_2, CO_2, CH_4, and H_2O (Eq. (12)).

$$\frac{\partial T_G}{\partial t} + \frac{\partial (T_G\, w_x)}{\partial x} - \sum_j \frac{\left(-\Delta H_{R,j} r_j \rho_C\right)}{\rho_G c_{p,G}} = 0 \tag{11}$$

$$\frac{\partial c_i}{\partial t} + \frac{\partial (c_i\, w_x)}{\partial x} - \sum_j \nu_{i,j}\, r_j \rho_C = 0 \tag{12}$$

The index *i* denotes the gas species. The index *j* describes the reactions: *j* = 1 for CO methanation, *j* = 2 for reverse water-gas shift reaction. As deduced in Sect. 3, the rates of reaction are defined as a Langmuir-Hinshelwood type and are taken from Klose formulated for an 18 % nickel catalyst and Zhang, respectively (Eqs. (6) and (8)). The equilibrium constants K_{METH} and K_{WGS} in the rate equations (Eqs. (6) and (8)) are calculated in dependence of temperature according to Elnashaie and Elshishini [39]. Heat losses and pressure drops were neglected in the reactor model.

For solving the set of partial differential equations, the equations were transformed to ordinary differential equations using an upwind differencing scheme [40]. To handle the ordinary differential equations, an implicit second-order backwards differencing solver with time step adaption (fixed-leading coefficient method [41]) was implemented and applied.

4.2 Simulation Frame Conditions

The simulation was performed for a fixed-bed reactor matching the typical size of plants producing biomass derived syngas (cf. [15]) or H_2/CO_2 mixtures coming from electrolysis plants operated with wind power (cf. [2, 16]); see Tab. 3.

Table 3. Reactor dimensions and catalyst loading used in the simulation model [33].

Parameter	Value
Reactor length [m]	2.00
Reactor diameter [m]	0.45
Catalyst loading [kg]	1190

As an exemplary CO methanation process, educt gas characteristics from the ADAM I test plant were taken, which is described by Harms [33]. Tab. 4 gives an overview of those characteristics.

Table 4. Educt characteristics of CO methanation used in the simulation model [33].

Parameter	Value
Pressure [bar]	27.2
Temperature [°C]	300
Volume flow [m^3h^{-1}] (STP)	1416 (STP)
Hourly space velocity [h^{-1}]	4454 (STP)
Carbon dioxide [vol %]	6.13
Carbon monoxide [vol %]	4.28
Methane [vol %]	28.12
Hydrogen [vol %]	36.88
Nitrogen [vol %]	5.41
Water steam [vol %]	19.18

For the simulation of an exemplary CO_2 methanation process, the educt gas pressure, temperature, volume flow, and composition are adapted from a typical CO_2 methanation process taken from [16]. They are listed in Tab. 5.

To prove the chosen rate equations for the application to dynamic modeling and simulation, the educt gas volume flow was increased stepwise by a factor of 1.25 (educt gas step) after the process has reached steady operation. Thereby, the educt gas composition, pressure, and temperature remain constant.

4.3 Simulation Results

The dynamic, i.e., time-dependent, simulation was used to calculate the response of the educt gas step. The results are presented in Fig. 6 which displays the educt gas volume flows of CO and CO_2 methanation as well as the corresponding meth-

Table 5. Educt gas characteristics of CO_2 methanation used in the simulation model [16].

Parameter	Value
Pressure [bar]	20.00
Temperature [°C]	400.00
Volume flow [m^3h^{-1}]	635.85 (STP)
Hourly space velocity [h^{-1}]	2000.00 (STP)
Carbon dioxide [vol %]	4.90
Carbon monoxide [vol %]	0
Methane [vol %]	45.48
Hydrogen [vol %]	19.60
Nitrogen [vol %]	0
Water steam [vol %]	30.00

ane volume flows at the reactor outlet over time. According to Fig. 6, the educt gas step shifts the system from a steady state to another. Each state is characterized by a constant methane volume flow over a period of time. By the CO methanation process, a methane volume flow of 544 m^3h^{-1} (STP) is provided before the step and 680 m^3h^{-1} (STP) after the step. Corresponding values of 316 m^3h^{-1} (STP) and 396 m^3h^{-1} (STP) are reached by the CO_2 methanation process. The respective increase of the methane volume flows between the two steady states are linear to the step (step factor: 1.25). Regarding the gas temperature, both, the CO and CO_2 methanation process, exhibit constant temperature profiles inside the reactor over time. The reason is a constant educt gas composition and temperature before and after the step at the reactor inlet.

In contrast to the sharp form of the educt gas steps, the methane volume flows show a gradually increasing curve as response before the steady state after the step. This is caused by

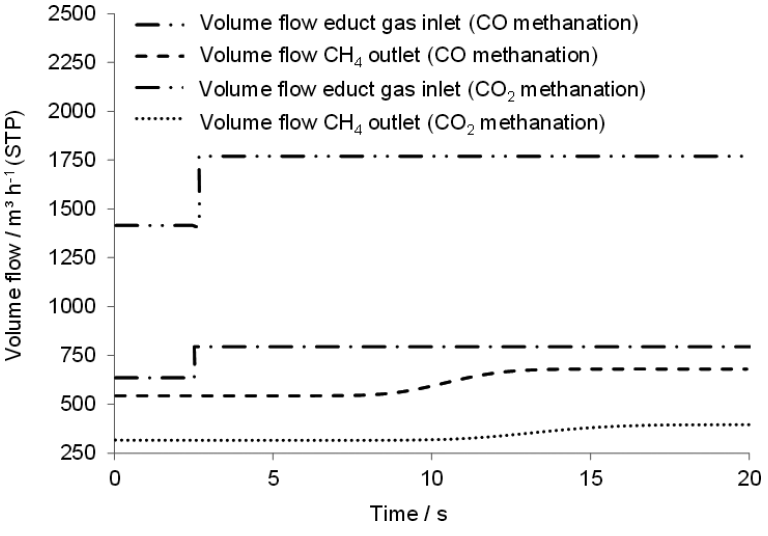

Figure 6. Simulated response of the educt gas step. Educt gas volume flow at reactor inlet and methane volume flow at reactor outlet in dependence of time for CO and CO_2 methanation.

numerical errors from the upwind discretization scheme used for the transformation of the partial differential equations to ordinary ones (see [42]).

Fig. 7 illustrates the simulated methane and CO volume flows over the reactor length for the CO methanation process. Additionally, the temperature course is presented. The simulation results displayed in Fig. 7 state the experimental data reported by Harms [33] (temperature reactor outlet: 604 °C; methane flow reactor outlet: 530 m^3h^{-1}) for similar conditions in terms of reactor dimensions, educt gas characteristics, etc. and validate the chosen reaction rates for CO methanation process modeling. The simulated CO conversion occurs within the first centimeters of the methanation reactor and the gas leaves the reactor close to the chemical equilibrium (temperature reactor outlet: 593 °C; methane flow reactor outlet: 544 m^3h^{-1}). A simplified Aspen Plus model was employed to estimate the equilibrium temperature for comparison (595 °C). Due to the exothermal character of the methanation reaction, the CO conversion and respective methane formation are accompanied by a significant temperature increase inside the reactor up to approximately 593 °C. As expected for an adiabatic reactor model, this temperature remains constant over the reactor length.

Also the results of the CO_2 methanation modeling (Fig. 8) confirm measurements from other authors (cf. [16]). As for CO methanation, the CO conversion occurs within the first reactor centimeters. However, due to a less reactive educt (CO_2) the reaction is slower than for CO methanation, compared with respect to the hourly space velocity).

5 Summary

The presented work can be summarized as follows:

- A multitude of kinetic approaches for the CO methanation over nickel catalysts was published within the last decades. However, only a few approaches rely on wide temperature and pressure ranges, which are prevalent for modern methanation applications, e.g., power-to-gas or biomass-based polygeneration plants. Especially the approaches of Xu [23] and Kopyscinski [19], which are frequently used for simulation-based methanation case studies, do not lead to satisfying results in typical fixed-bed methanation temperature ranges between 300 °C and 600 °C.
- Due to legal restrictions regarding the publication of kinetic data for commercial nickel catalysts, the choice of an appropriate kinetic approach for the simulation-based design and control of methanation plants operating with commercial catalysts is difficult. Despite of manifold differences of the applied catalysts, e.g., promoters and pore structure, their nickel content can be an indicator for the choice of a kinetic approach.
- The comparison of different kinetic approaches determined at elevated pressures with commercial methanation catalysts helps to identify two

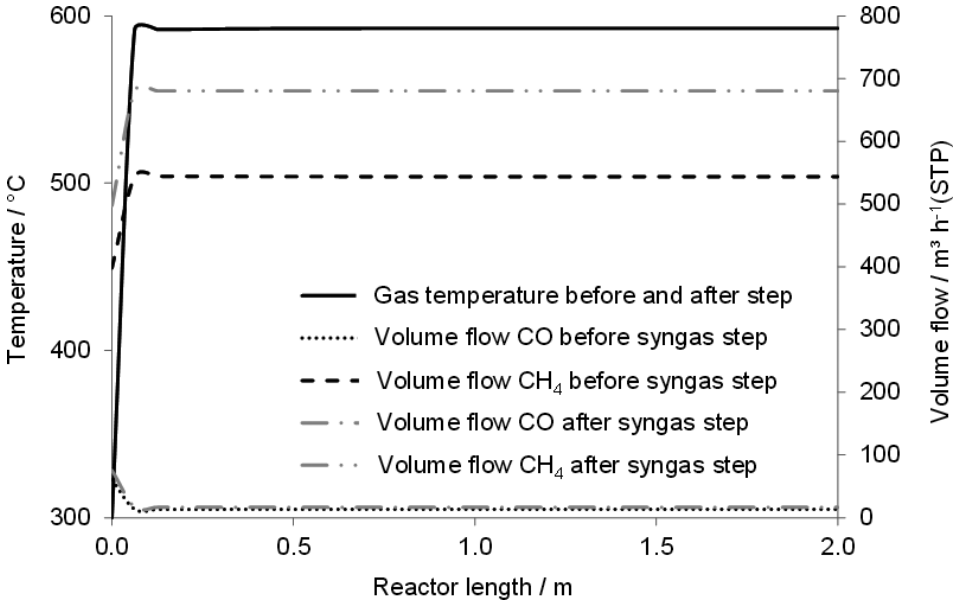

Figure 7. Results of dynamic CO methanation simulation. Temperature and gas (CO, CH_4) volume flows over the reactor length before and after educt gas step.

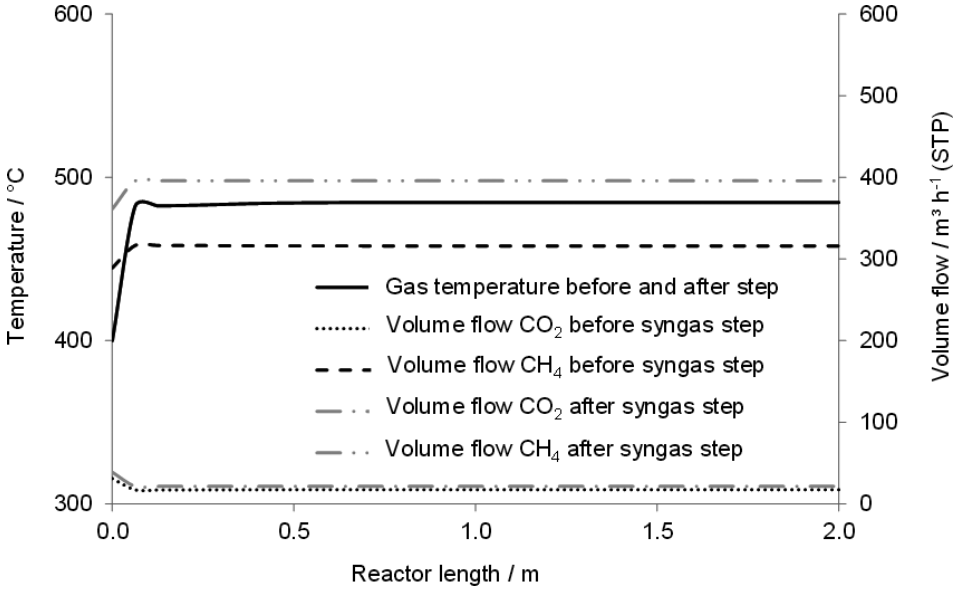

Figure 8. Results of dynamic CO_2 methanation simulation. Temperature and gas (CO_2, CH_4) volume flows over the reactor length before and after educt gas step.

different kinetic approaches for the modeling and dynamic simulation of methanation plants with commercial 18 % and 50 % nickel catalysts at varying temperatures and pressures. Own measurements confirm this assumption. For commercial catalysts with 18 % nickel the reaction rate published by Klose [26] is appropriate. For catalysts with 50 % nickel the rate published by Zhang [29] is suitable.

– For the modeling of CO_2 methanation processes in addition to the rate of CO methanation a second reaction rate is necessary. As the reaction equation of the CO_2 methanation is a linear combination of CO methanation and reverse water-gas shift reaction, a rate for the reverse water-gas shift reaction should be complemented. However, most kinetic studies on CO methanation neglect the reverse water-gas shift reaction.

– The analysis shows that the rate for the reverse water-gas shift reaction published by Xu [23] is not suitable at temperatures below 500 °C typically related to state-of-the-art methanation processes. But, data reported by Zhang [29] match actually published measurements of CO_2 methanation. This was confirmed by a dynamic simulation with a 1D fixed-bed reactor model.

The authors have declared no conflict of interest.

Symbols used

c_i	$[\mathrm{mol\,m^{-3}}]$	concentration gas component *i*
$c_{p,G}$	$[\mathrm{J\,kg^{-1}K^{-1}}]$	specific heat capacity gas

E_1	[J mol^{-1}]	activation energy CO methanation
E_2	[J mol^{-1}]	activation energy water-gas shift reaction
$\Delta H_{R,j}$	[J mol^{-1}]	heat of reaction j
ΔH_C	[J mol^{-1}]	enthalpy of adsorption C
ΔH_H	[J mol^{-1}]	enthalpy of adsorption H
ΔH_{CO}	[J mol^{-1}]	enthalpy of adsorption CO
ΔH_{H_2}	[J mol^{-1}]	enthalpy of adsorption H_2
ΔH_{CH_4}	[J mol^{-1}]	enthalpy of adsorption CH_4
ΔH_{H_2O}	[J mol^{-1}]	enthalpy of adsorption H_2O
k_1	[mol kg^{-1}cat. s^{-1}]	rate coefficient CO methanation
k_2	[mol kg^{-1}cat. s^{-1}bar^{-1}]	rate coefficient water-gas shift reaction
k_1^0	[mol kg^{-1}cat. s^{-1}]	preexponential factor of rate coefficient k_1
k_2^0	[mol kg^{-1}cat. s^{-1}bar^{-1}]	preexponential factor of rate coefficient k_2
K_{METH}	[bar^2]	equilibrium constant CO methanation
K_{WGS}	[–]	equilibrium constant water-gas shift reaction
K_C	[bar$^{-0.5}$]	adsorption constant C
K_{CH_4}	[bar^{-1}]	adsorption constant CH_4
K_{CO}	[bar^{-1}]	adsorption constant CO
K_H	[bar$^{-0.5}$]	adsorption constant H
K_{H_2}	[bar^{-1}]	adsorption constant H_2
K_{H_2O}	[–]	adsorption constant H_2O
K_C^0	[bar$^{-0.5}$]	preexponential factor of adsorption constant C
K_H^0	[bar$^{-0.5}$]	preexponential factor of adsorption constant H
K_{CO}^0	[bar^{-1}]	preexponential factor of adsorption constant CO
$K_{H_2}^0$	[bar^{-1}]	preexponential factor of adsorption constant H_2
$K_{CH_4}^0$	[bar^{-1}]	preexponential factor of adsorption constant CH_4
$K_{H_2O}^0$	[–]	preexponential factor of adsorption constant H_2O
p	[bar]	pressure
p_i	[bar]	partial pressure of gas component i
r_j	[mol kg^{-1}cat. s^{-1}]	rate of reaction j
t	[s]	time
T_G	[K]	gas temperature
w_x	[m s^{-1}]	gas velocity in direction x
x	[m]	x-coordinate (in gas flow direction)
y	[–]	mole fraction

Greek letters

$\nu_{i,j}$	[–]	stoichiometric coefficient gas component i in reaction j
ρ_C	[kg m^{-3}]	bulk density catalyst
ρ_G	[kg m^{-3}]	density gas

Abbreviations

METH	methanation
MFC	mass flow controller
SNG	synthetic natural gas
STP	standard temperature and pressure
WGS	water-gas shift

References

[1] M. Götz, S. Bajohr, F. Graf, R. Reimert, T. Kolb, *Chem. Ing. Tech.* **2013**, *85*, 1146–1151.
[2] S. Schiebahn, T. Grube, M. Robinius, V. Tietze, B. Kumar, D. Stolten, *Int. J. Hydrogen Energy* **2015**, *40*, 4285–4294.
[3] M. Götz, S. Bajohr, D. Buchholz, *Energ. | Wasser Prax.* **2011**, *62*, 72–76.
[4] S. Rönsch, M. Zeymer, S. Majer, *Chem. Ing. Tech.* **2014**, *86*, 1678–1689.
[5] J. Lefebvre, M. Götz, S. Bajohr, R. Reimert, T. Kolb, *Fuel Process. Technol.* **2015**, *132*, 83–90.
[6] S. Rönsch, S. Matthischke, M. Müller, P. Eichler, *Chem. Ing. Tech.* **2014**, *86*, 1198–1204.
[7] P. Sabatier, J.-B. Senderens, *Comptes Rendus Des Séances De L'Académie Des Sciences, Section VI – Chimie*, Imprimerie Gauthier-Villars, Paris **1902**.
[8] H. Hiller, R. Reimert, H.-M. Stönner, in *Ullmann's Encyclopedia of Industrial Chemistry*, Wiley-VCH Verlag, Weinheim **2006**, 20.
[9] J. Kopyscinski, T. J. Schildhauer, S. M. A. Biollaz, *Fuel* **2010**, *89*, 1763–1783.
[10] S. Rönsch, A. Ortwein, *Chem. Ing. Tech.* **2011**, *83*, 1200–1208.
[11] K. Kaltenmaier, *Ph. D. Thesis*, Universität Karlsruhe (TH) **1988**.
[12] G. D. Weatherbee, C. H. Bartholomew, *J. Catal.* **1982**, *77*, 460–472.
[13] H. Hiller, R. Reimert, in *Ullmann's Encyclopedia of Industrial Chemistry*, Wiley-VCH Verlag, Weinheim **2006**, 10.
[14] B. Rehling, H. Hofbauer, R. Rauch, C. Aichernig, *Biomass Convers. Biorefin.* **2011**, *1*, 111–119.
[15] S. Rönsch, M. Kaltschmitt, *Biomass Convers. Biorefin.* **2012**, *2*, 285–296.
[16] T. Schaaf, J. Grünig, M. R. Schuster, T. Rothenfluh, A. Orth, *Energy Sustain. Soc.* **2014**, *4*. DOI: 10.1186/s13705-014-0029-1
[17] S. Matthischke, S. Rönsch, *Proceedings of the DGMK-Fachbereichstagung Konversion von Biomassen*, Rotenburg a.d. Fulda **2014**.
[18] M. Götz, F. Ortloff, R. Reimert, O. Basha, B. I. Morsi, T. Kolb, *Energy Fuels* **2013**, *27*, 4705–4716.
[19] J. Kopyscinski, *Ph. D. Thesis*, ETH Zürich **2010**.
[20] G. A. Mills, F. W. Steffgen, *Catal. Rev. Sci. Eng.* **1974**, *8*, 159–210.
[21] J. Klose, *Ph. D. Thesis*, Ruhr-Universität Bochum **1982**.
[22] M. A. Vannice, *Cat. Rev. Sci. Eng.* **1976**, *14*, 153–191.
[23] J. Xu, G. F. Froment, *AIChE J.* **1989**, *35*, 88–96.
[24] P. Schoubye, *J. Catal.* **1969**, *14*, 238–246.
[25] E. L. Sughrue, C. H. Bartholomew, *Appl. Catal.* **1982**, *2*, 239–256.

[26] J. Klose, M. Baerns, *J. Catal.* **1984**, *85*, 105–116.
[27] R. E. Hayes, W. J. Thomas, K. E. Hayes, *J. Catal.* **1985**, *92*, 312–326.
[28] Y.-W. Chen, *J. Eng.* **1988**, *1*, 7–18.
[29] J. Zhang, N. Fatah, S. Capela, Y. Kara, O. Guerrini, A. Y. Khodakov, *Fuel* **2013**, *111*, 845–854.
[30] S. V. Ho, P. Harriot, *J. Catal.* **1980**, *64*, 272–283.
[31] D. Schlereth, O. Hinrichsen, *Chem. Eng. Res. Des.* **2014**, *92*, 702–712.
[32] R. Güttel, *Chem. Eng. Technol.* **2013**, *36*, 1675–1682.
[33] H. Harms, B. Höhlein, A. Skov, *Chem. Ing. Tech.* **1980**, *52*, 504–515.
[34] J. R. Rostrup-Nielsen, K. Pedersen, J. Sehested, *Appl. Catal., A* **2007**, *330*, 134–138.
[35] J. Sehested, S. Dahl, J. Jacobsen, J. R. Rostrup-Nielsen, *J. Phys. Chem. B* **2005**, *109*, 2432–2438.
[36] M. Götz, *Ph. D. Thesis*, Karlsruher Institut für Technologie **2014**.
[37] J. Köchermann, J. Schneider, S. Matthischke, S. Rönsch, *Fuel Process. Technol.* **2015**, *138*, 37–41.
[38] S. Rönsch, *Anlagenbilanzierung in der Energietechnik – Grundlagen, Gleichungen und Modelle für die Ingenieurpraxis*, 1st ed., Springer Vieweg, Wiesbaden **2015**, 264.
[39] S. Elnashaie, S. Elshishini, *Modelling, Simulation and Optimization of Industrial Fixed Bed Catalytic Reactors*, 1st ed., Yverdon, Gordon and Breach Science Publishers, Yverdon, Langhorne **1993**, 62.
[40] S. Rönsch, *Anlagenbilanzierung in der Energietechnik – Grundlagen, Gleichungen und Modelle für die Ingenieurpraxis*, 1st ed., Springer Vieweg, Wiesbaden **2015**, 335.
[41] R. Sacks-Davis, *ACM Trans. Math. Software* **1980**, *6*, 540–562.
[42] P. V. Danckwerts, *Chem. Eng. Sci.* **1953**, *2*, 1–13.

